

MEASURING EJECTA VELOCITY IMPROVES TYPE IA SUPERNOVA DISTANCES

RYAN J. FOLEY^{1,2} AND DANIEL KASEN^{3,4}

Draft version November 5, 2018

ABSTRACT

We use a sample of 121 spectroscopically normal Type Ia supernovae (SNe Ia) to show that their intrinsic color is correlated with their ejecta velocity, as measured from the blueshift of the Si II $\lambda 6355$ feature near maximum brightness, $v_{\text{Si II}}$. The SN Ia sample was originally used by Wang et al. (2009) to show that the relationship between color excess and peak magnitude, which in the absence of intrinsic color differences describes a reddening law, was different for two subsamples split by $v_{\text{Si II}}$ (defined as “Normal” and “High-Velocity”). We verify this result, but find that the two subsamples have the same reddening law when extremely reddened events ($E(B - V) > 0.35$ mag) are excluded. We also show that (1) the High-Velocity subsample is offset by ~ 0.06 mag to the red from the Normal subsample in the $(B_{\text{max}} - V_{\text{max}}) - M_V$ plane, (2) the $B_{\text{max}} - V_{\text{max}}$ cumulative distribution functions of the two subsamples have nearly identical shapes, but the High-Velocity subsample is offset by ~ 0.07 mag to the red in $B_{\text{max}} - V_{\text{max}}$, and (3) the bluest High-Velocity SNe Ia are ~ 0.10 mag redder than the bluest Normal SNe Ia. Together, this evidence indicates a difference in intrinsic color for the subsamples. Accounting for this intrinsic color difference reduces the scatter in Hubble residuals from 0.190 mag to 0.130 mag for SNe Ia with $A_V \lesssim 0.7$ mag. The scatter can be further reduced to 0.109 mag by exclusively using SNe Ia from the Normal subsample. Additionally, this result can at least partially explain the anomalously low values of R_V found in large SN Ia samples. We explain the correlation between ejecta velocity and color as increased line blanketing in the High-Velocity SNe Ia, causing them to become redder. We discuss some implications of this result, and stress the importance of spectroscopy for future SN Ia cosmology surveys, with particular focus on the design of WFIRST.

Subject headings: supernovae: general — distance scale — dust, extinction

1. INTRODUCTION

Type Ia supernovae (SNe Ia) are very good distance indicators after making an empirical correction based on their light-curve shape and color (Phillips 1993; Riess et al. 1996). The distances are precise enough to determine that the expansion of the Universe is accelerating (Riess et al. 1998; Perlmutter et al. 1999), and constrain the equation-of-state parameter of Dark Energy (Astier et al. 2006; Wood-Vasey et al. 2007; Riess et al. 2007; Hicken et al. 2009b; Kessler et al. 2009; Amanullah et al. 2010). The current best precision is 0.15 and 0.11 mag in absolute magnitude (after corrections) when using optical information only and combining it with near-infrared data, respectively (Mandel et al., in prep.), although most samples have a precision of ~ 0.17 mag (e.g., Hicken et al. 2009a).

Since peak luminosity, light-curve shape, intrinsic color, and most spectral parameters all correlate with each other and with measured ^{56}Ni mass (e.g., Nugent et al. 1995; Stritzinger et al. 2006), measuring the light-curve shape of a SN Ia is adequate to determine its peak luminosity. Observing a SN Ia in multiple passbands allows one to estimate its reddening. Therefore with only light curves in a few passbands, one can precisely measure the distance to a SN Ia.

However, as mentioned above, the precision in measuring the distance modulus of an individual SN Ia has a floor of 0.15 mag when observing (rest-frame) optical passbands. There have been many attempts to further reduce the Hubble scatter with a “second parameter” that does not strongly correlate with other luminosity indicators. In particular, since spectra must contain more information than light curves, several investigations have looked for correlations between spectral parameters and both light-curve shape and Hubble residuals, with most correlations between spectral parameters and light-curve shape not improving the Hubble scatter. However, two studies have been able to make a further reduction to the Hubble scatter using the ratios of fluxes at particular wavelengths (Foley et al. 2008; Bailey et al. 2009), but both require further data to verify the results and a theoretical understanding of why particular wavelengths have such power.

Benetti et al. (2005) showed that although a single parameter can adequately account for the variation in the peak luminosity, light-curve shape, and temperature of SNe Ia, the velocity gradient of the Si II $\lambda 6355$ feature, $\dot{v}_{\text{Si II}}$, is not well correlated with these other observables. The Si II $\lambda 6355$ feature, being relatively strong and isolated in maximum-light spectra, is the hallmark feature of SNe Ia (for a review of SN spectroscopy, see Filippenko 1997). Benetti et al. (2005) separated their sample of SNe Ia into three groups: high-velocity gradient (HVG) objects, consisting of SNe Ia with $\dot{v}_{\text{Si II}} \gtrsim 70 \text{ km s}^{-1} \text{ day}^{-1}$ and $\Delta m_{15}(B) \lesssim 1.5$ mag, low-velocity gradient (LVG) objects, consisting of SNe Ia with $\dot{v}_{\text{Si II}} \lesssim 70 \text{ km s}^{-1} \text{ day}^{-1}$ and $\Delta m_{15}(B) \lesssim 1.5$ mag,

¹ Harvard-Smithsonian Center for Astrophysics, 60 Garden Street, Cambridge, MA 02138.

² Clay Fellow. Electronic address rfoley@cfa.harvard.edu .

³ Department of Physics, University of California at Berkeley, 366 LeConte, Berkeley, CA 94720.

⁴ Nuclear Science Division, Lawrence Berkeley National Laboratory, Berkeley, CA 94720.

and FAINT objects which have $\Delta m_{15}(B) \gtrsim 1.5$ mag. The HVG and LVG subsamples have similar light-curve shape, peak luminosity, and color demographics. Finally, Benetti et al. (2005) found that HVG SNe Ia tended to have a higher velocity for the Si II feature near maximum than the LVG SNe Ia.

Wang et al. (2009), hereafter W09, presented an analysis of 158 spectroscopically normal SNe Ia (i.e., “Branch-normal” objects; Branch et al. 1993; which excludes SNe Ia similar to SN 1991T; Filippenko et al. 1992b; Jeffery et al. 1992; SN 1991bg; Filippenko et al. 1992a; Leibundgut et al. 1993; and more peculiar SNe Ia; e.g., SN 2000cx; Li et al. 2001; SN 2002cx; Li et al. 2003; SN 2003fg; Howell et al. 2006; SN 2008ha; Foley et al. 2009), which were separated by their Si II $\lambda 6355$ velocity near maximum light, $v_{\text{Si II}}$. They showed that this selection was essentially equivalent to using $\dot{v}_{\text{Si II}}$ for the SNe Ia where there was a good spectroscopic sequence. SNe Ia above and below a velocity of $\sim 11,800 \text{ km s}^{-1}$ were classified as “High-Velocity” and “Normal” SNe Ia⁵, respectively. They looked at the correlation between color excess (essentially an offset from maximum-light $B - V$ color) and peak absolute magnitude corrected for light-curve shape, but not for color. If the color excess is truly the result of dust, this relationship is between color excess and extinction, and the slope of a line fit to the relationship should provide a measurement of the ratio of total to selective extinction, $A_V/E(B - V) = R_V$. The objects within the two subsamples follow a different relation between peak absolute magnitude (again, uncorrected for color) and color excess, indicating different values of R_V for the two subsamples: $R_V = 2.36$ and 1.37 for the Normal and High-Velocity subsamples, respectively. Both of these values, are significantly less than the Milky Way value of $R_V = 3.1$.

Kasen & Plewa (2007), hereafter KP07, presented theoretical light curves and spectra of a SN Ia model from several different viewing angles. The ejecta in the model were asymmetric such that different viewing angles had different values for $\dot{v}_{\text{Si II}}$ and $v_{\text{Si II}}$ but similar values of $\Delta m_{15}(B)$ and peak magnitude. Since it was the same explosion model, all generated light curves and spectra come from an event with a single total energy and ^{56}Ni mass. Although the details of the model presented by KP07 may not properly describe SNe Ia, the generic attributes of the observables are useful when discussing differences in ejecta velocity for SNe Ia with similar peak luminosity and/or light-curve shape.

Although neither study focused on this result, both W09 and KP07 found correlations between $v_{\text{Si II}}$ and the $B - V$ color of the SN at maximum light. W09 found a ~ 0.1 mag offset between $B - V$ colors of the Normal and High-Velocity subsamples. KP07 showed that both $B - V$ color and $v_{\text{Si II}}$ depend on the viewing angle of their asymmetric two-dimensional model.

This manuscript examines the correlation of color with ejecta velocity. It attempts to explain the physical cause of the correlation and examines the implications for measuring SN Ia distances. We suggest that a single

maximum-light spectrum will significantly improve the precision of the measured distance for a given SN Ia. In Section 2, we re-analyze the W09 sample, examining in detail the relationship between these quantities. We find that the intrinsic color of a SN Ia at maximum brightness depends on the velocity of the ejecta. We also show that a proper treatment of the intrinsic colors of SNe Ia with different ejecta velocities can significantly improve the precision of distance measurements. In Section 3, we provide a simple theoretical explanation for our results as well as examine more complex models. In Section 4, we summarize our results and discuss their implications for future studies.

2. EJECTA VELOCITY AND INTRINSIC COLOR

As discussed above, W09 presented an analysis of 158 SNe Ia that concluded that separating the objects into two subsamples based on $v_{\text{Si II}}$ and treating their extinction corrections differently will reduce the scatter of their Hubble residuals. In this section, we re-analyze the data presented by W09, showing that their analysis stands. However, (1) a different R_V for the two subsamples is only necessary when including the reddest events, (2) for SNe Ia with $E(B - V) \leq 0.3$ mag, both subsamples have reddening laws consistent with $R_V = 3.1$, (3) there is a clear offset in the color of SNe Ia in the two subsamples, (4) separating the objects into two subsamples can partially account for the low R_V values measured for large samples of low-reddening SNe Ia, and (5) using this difference in color, one can significantly reduce the scatter of the Hubble residuals for these SNe Ia.

From the entire W09 sample, we remove SN 2006bt, which has spectral and photometric peculiarities that result in a peak luminosity fainter than its light-curve shape would suggest (Foley et al. 2010). Like W09, we remove SN 2006lf, which has a Milky Way reddening of $E(B - V) = 0.97$ mag and was ~ 0.7 mag brighter than that of a typical SN Ia after light-curve shape correction. To avoid large systematic uncertainties for the peak absolute magnitudes, W09 excluded all SNe with $z < 0.01$ that do not have a Cepheid distances from their final analysis. We also remove these objects from our sample. After making these cuts, 121 SNe Ia remain in the final sample, with 81 and 40 SNe Ia being in the Normal and High-Velocity subsamples, respectively.

2.1. Verification of Previous Analysis

To verify the results of W09, we examine their sample of SNe Ia in the same manner as W09. In particular, we use Equation 1 of W09:

$$M_{\text{max}}^V = M_{\text{zp}} + \alpha(\Delta m_{15}(B) - 1.1) + R_V E(B - V)_{\text{host}}. \quad (1)$$

This two-component fit is similar to the two-component fit used by Tripp (1998) and in the SALT (Guy et al. 2005, 2007) and SiFTO (Conley et al. 2008) light-curve fitters.

W09 provides all necessary information in their Table 1. Fitting the data, we find the same values for M_{zp} , α , and R_V as W09: -19.26 mag, 0.77 , and 2.36 ; and -19.28 mag, 0.75 , and 1.58 for the Normal and High-Velocity SNe Ia, respectively. After fixing $\alpha = 0.75$ (similar to W09), we refit the data, finding slightly different values for R_V (2.48 ± 0.11 and 1.63 ± 0.08 for Normal and High-Velocity SNe Ia, respectively). These values

⁵ We use “Normal” to describe these objects since W09 used this terminology. But we caution that it could be confused with “Branch normal,” which both Normal and High-Velocity SNe Ia are considered. Calling these objects “Low-Velocity” in the future may reduce this potential confusion.

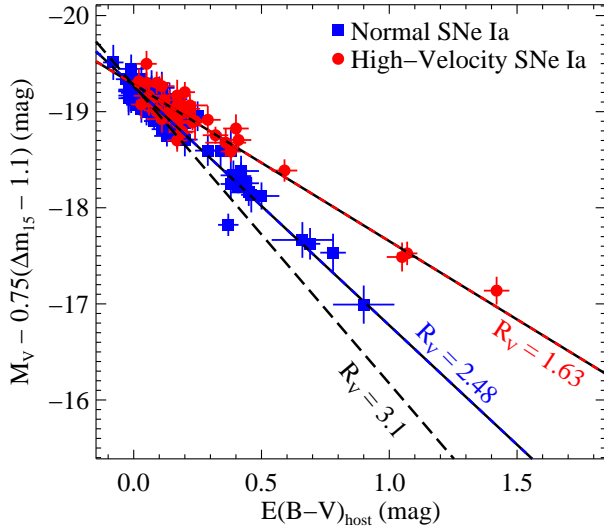


FIG. 1.— Our re-creation of Figure 4 of W09. The light-curve shape corrected peak absolute V brightness as a function of host color excess. The blue squares and red circles represent the Normal and High-Velocity SNe Ia, respectively. The best fit lines for each subsample correspond to $R_V = 2.48$ and 1.63 for the Normal and High-Velocity SNe Ia (corresponding to blue-black and red-black dashed lines), respectively. The Milky Way reddening law of $R_V = 3.1$ is also shown as the dashed line.

differ very slightly (and within the uncertainties) from those found by W09. Figure 1 presents our recreation of Figure 4 from W09.

From Figure 1, it is clear that the subsamples have different relationships between color excess and peak absolute magnitude after correcting for light-curve shape. Similarly, both subsamples have reddening laws different from that of the Milk Way. However, a closer examination of the data is required.

2.2. Excluding the Reddest Supernovae

As noted by W09, the reddening laws for the two groups are significantly different even if SNe Ia with $E(B - V)_{\text{host}} > 0.5$ mag are excluded from the fit. However, SNe Ia with $E(B - V)_{\text{host}} = 0.5$ mag are highly reddened objects (corresponding to $0.8 \leq A_V \leq 1.6$ mag depending on R_V). These SNe Ia are very rarely seen at high redshift and only occasionally observed in the local universe. In fact, the only high- z SN Ia in the Constitution set of SNe Ia (Hicken et al. 2009b) with $E(B - V) > 0.5$ mag is from the Higher- z *HST* survey (Riess et al. 2007) and has $E(B - V)_{\text{host}} = 0.52$ mag. This object is also at $z = 0.216$, making it the lowest-redshift SN Ia of the *HST*-discovered SNe Ia. For current cosmological analyses, this color limit is not particularly useful.

In Figure 2, we again present the data of W09, except now we only show the data with $E(B - V)_{\text{host}} < 0.35$ mag (corresponding to $A_V < 0.57$, 0.87 , and 1.09 mag for $R_V = 1.63$, 2.48 , and 3.1 , respectively). For all further analysis, the light-curve shape parameter, α , is fixed at 0.75 . As a check, we have also performed all analysis leaving this as a free parameter, and it is always consistent with 0.75 . However, for subsamples with a small number of SNe Ia the uncertainty for the parameter can

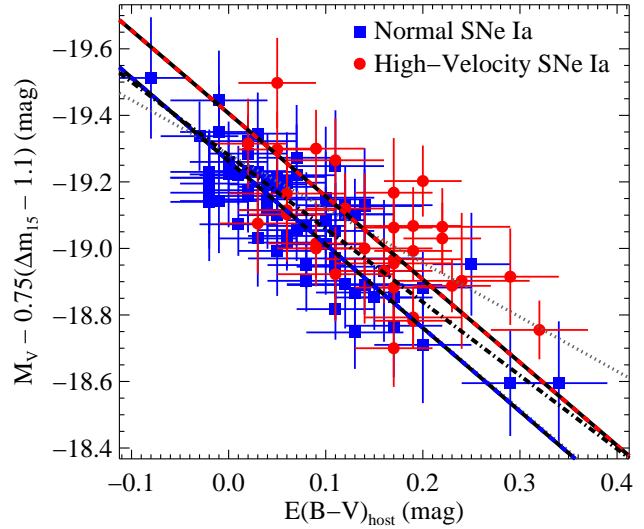


FIG. 2.— Same as Figure 1, except for SNe Ia with $E(B - V)_{\text{host}} < 0.35$ mag. The best-fit lines for the restricted subsamples are shown as blue-black and red-black dashed lines and correspond to $R_V = 2.51$ and 2.50 for the Normal and High-Velocity SNe Ia, respectively. The best-fit lines for the full subsamples (as shown in Figure 1) are shown as grey dotted lines and correspond to $R_V = 2.48$ and 1.63 for the Normal and High-Velocity SNe Ia, respectively; however, the line for the Normal subsample is almost completely covered by the line fit to the low reddening Normal SNe Ia. A fit to the full sample of SNe Ia with $E(B - V)_{\text{host}} < 0.35$ mag is shown as a dot-dashed line and corresponds to $R_V = 2.21$.

be large, and fixing the parameter for all fits makes comparing samples more direct and convenient. For the subsample with $E(B - V)_{\text{host}} < 0.35$ mag, the data produces best-fit values of $(M_{\text{zp}}, R_V) = (-19.26 \pm 0.03 \text{ mag}, 2.51 \pm 0.28)$ and $(-19.41 \pm 0.08 \text{ mag}, 2.50 \pm 0.47)$ for Normal and High-Velocity SNe Ia, respectively. The fit parameters for the low-reddening Normal subsample are consistent with those founds for the entire Normal subsample. Conversely, the low-reddening High-Velocity subsample has values of M_{zp} and R_V that differ at the 1.5 and 1.8σ level from those found for the entire High-Velocity subsample. Although these differences are not statistically significant, the 0.12 mag offset in absolute magnitude and 0.87 offset in R_V (corresponding to a difference of 0.17 mag in A_V for $E(B - V) = 0.2$ mag) can dramatically affect the implied distances of SNe Ia at cosmological distances.

We further examine this difference by fitting all data with $E(B - V)_{\text{host}}$ below a certain ceiling and varying that maximum value. The resulting best-fit parameters are shown in Figure 3. Naturally, the uncertainties for M_{zp} and R_V are much larger for a smaller $E(B - V)_{\text{max}}$. This is both because of a smaller number of SNe Ia in each subsample and the smaller lever arm for fitting the line. Regardless, the two subsamples always have consistent values of M_{zp} ; however, they are only consistent at the $\sim 1\sigma$ level for $E(B - V)_{\text{max}} < 0.4$ mag. (Section 2.3 shows that this is likely an offset in color rather than in peak absolute magnitude.) The two subsamples also have consistent values for R_V for $E(B - V)_{\text{max}} < 0.4$ mag, but deviate significantly for higher values (W09). Additionally, both subsamples are consistent with $R_V = 3.1$ (at

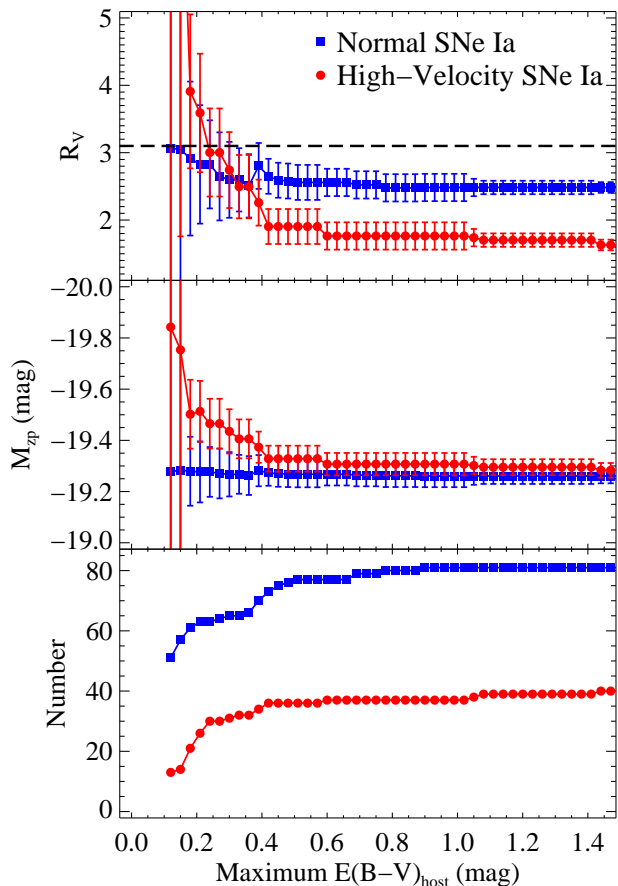


FIG. 3.— Best-fit R_V (first panel) and M_{zp} (second panel), as well as the number of SNe in each subsample (third panel) as a function of maximum $E(B - V)_{\text{host}}$. The Normal and High-Velocity SNe Ia are represented by the blue squares and red circles, respectively. The dashed line in the first panel represents $R_V = 3.1$.

1σ) for $E(B - V)_{\text{max}} \leq 0.3$ mag.

The fit parameters do not change significantly for any subsample of Normal SNe Ia. But R_V changes significantly depending on the maximum reddening for the High-Velocity SNe Ia. It is possible that the highly reddened High-Velocity SNe Ia have a value of R_V that is significantly smaller than that of less reddened High-Velocity SNe Ia or any Normal SN Ia. A low value for R_V has been measured for individual High-Velocity SNe Ia (e.g., Krisciunas et al. 2000; Wang et al. 2008). We note that SN 2003cg, which is defined as a Normal object in the W09 sample, but is excluded from our analysis because of its redshift, was measured to have $R_V = 1.80$ (Elias-Rosa et al. 2006). Goobar (2008) suggested that a low value for R_V may be the result of multiple scatterings off circumstellar dust. In this scenario, it is natural that low values of R_V are associated with large values of $E(B - V)$. Although the possibility of circumstellar dust for all High-Velocity SNe Ia cannot strictly be ruled out, the higher value of R_V for the low-reddening sample suggests that it is not the dominant component of any extinction. Furthermore, as seen in Figure 2, there is an offset between the Normal and High-Velocity subsamples in the $M_V - E(B - V)_{\text{host}}$ plane that must be the result of some linear combination of M_V and $E(B - V)_{\text{host}}$. Therefore, the subsamples have intrin-

sically different light-curve shape-corrected peak luminosities (with the High-Velocity subsample being more luminous), have intrinsically different colors (with the High-Velocity subsample being redder), and/or intrinsically different dust distributions (with the High-Velocity subsample having more dust along the line of sight). The highly reddened SNe Ia probably have different properties from the low-reddening SNe Ia, with the highly reddened High-Velocity SNe Ia having a lower R_V than the low-reddening members of that subsample. Further investigations are necessary to determine (1) why highly reddened High-Velocity SNe Ia have a low value for R_V , and (2) if low-reddening SNe Ia have a value of R_V that is inconsistent with 3.1.

The results of restricting the samples by reddening show that the extremely reddened objects highly influence the fit parameters. Depending on choices made to cull the sample or (particularly for high- z) selection effects, these values may vary dramatically.

2.3. Color Offsets

By restricting the W09 sample to have $E(B - V)_{\text{host}} < 0.35$ mag, we found in Section 2.2 that the two velocity-selected subsamples have different magnitude zero points, M_{zp} . However, this is only one way to interpret the data; the other possibility is that there is an offset in $E(B - V)_{\text{host}}$ for the two subsamples. This is effectively shifting the lines in Figure 2 left-right rather than up-down. From the best-fit lines, the offset is ~ 0.06 mag.

To clearly see this effect, we look again at the data from W09. Instead of using the derived $E(B - V)_{\text{host}}$ values from W09, we use their values of $B_{\text{max}} - V_{\text{max}}$ (in most cases, there is a simple offset between the two values). This pseudo-color is simply the B magnitude at B_{max} minus the V magnitude at V_{max} , with no correction for host reddening. We also restrict the sample to SNe Ia with $1 \leq \Delta m_{15}(B) \leq 1.5$ mag and $B_{\text{max}} - V_{\text{max}} < 0.5$ mag. As noted by W09, the two subsamples have similar demographics over this range of $\Delta m_{15}(B)$.

W09 noted that for $B_{\text{max}} - V_{\text{max}} < 0.2$ mag there was a 0.08 mag offset (0.10 mag if restricting the $\Delta m_{15}(B)$ range) in the average $B_{\text{max}} - V_{\text{max}}$ between the two subsamples. There is also a lack of very blue ($B_{\text{max}} - V_{\text{max}} < -0.05$ mag) SNe Ia in the High-Velocity subsample. The bluest objects in a sample represent the lowest reddening and intrinsically bluest SNe Ia for that sample. For the Normal subsample to have several SNe Ia bluer than the bluest High-Velocity SN Ia, all High-Velocity SNe Ia must be significantly reddened and/or the High-Velocity and Normal SNe Ia have intrinsically different colors. In the top panel of Figure 4, Figure 1 is remade, except each SN Ia is plotted as a function of $B_{\text{max}} - V_{\text{max}}$ instead of $E(B - V)_{\text{host}}$ and only show SNe Ia with $1 \leq \Delta m_{15}(B) \leq 1.5$ mag. In the bottom panel of the figure, the same data are presented, except the High-Velocity SNe Ia are shifted by $B_{\text{max}} - V_{\text{max}} = -0.06$ mag, the value found from the best-fit lines.

Although by eye the overlap between the Normal and High-Velocity objects may not appear to be significantly different between the raw and shifted data, it is clear that the shifted data are a much better match to the bluest and reddest Normal SNe Ia than the raw data. That is, this simple shift adequately accounts for the lack of blue objects in the High-Velocity subsample and removes the

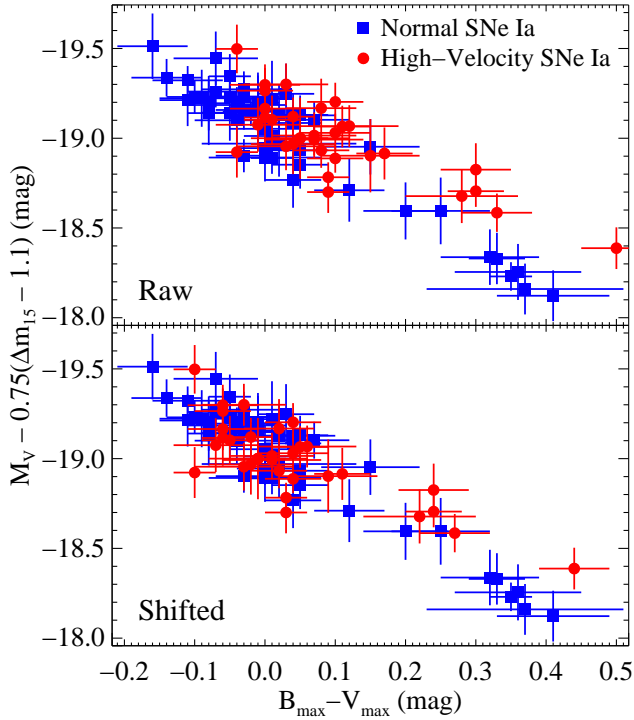


FIG. 4.— Same as Figure 2, except data are plotted as a function of $B_{\max} - V_{\max}$ and only SNe Ia with $1 \leq \Delta m_{15}(B) \leq 1.5$ mag are displayed. The top panel shows the raw data, while the bottom panel displays the same data with the High-Velocity subsample shifted by $B_{\max} - V_{\max} = -0.06$ mag.

overall offset in the two populations.

Another way to examine the effect of shifting the data is by examining the cumulative distribution functions (CDFs) for the subsamples. The CDFs for both subsamples are presented in Figure 5. Clearly, there is a dearth of blue SNe Ia in the High-Velocity subsample, with 26% of the Normal subsample being bluer than the bluest High-Velocity SN Ia. However, the overall shape of the CDFs for the Normal and High-Velocity subsamples are similar. After shifting the High-Velocity subsample by -0.07 mag, the CDFs are very similar except perhaps for the reddest part of the sample where dust extinction must be the dominant source of color differences. A simple Kolmogorov-Smirnov (K-S) test shows that there is a 0.65% chance that the Normal and High-Velocity objects have the same parent population. The Normal and shifted High-Velocity subsamples have a K-S probability of 99.99%, which does not mean that the subsamples have the same probability (especially since the High-Velocity colors were arbitrarily shifted by a fixed amount), but does show the outstanding agreement in the two subsamples' CDFs after the shift. The value of -0.07 mag was chosen to maximize the K-S probability, but values of -0.06 and -0.08 mag yield values of 73.07 and 98.96%, respectively.

As discussed in W09, the offset in maximum-light colors is likely the result of either different amounts of dust or intrinsically different colors. If the offset is primarily from dust, then the subsamples must have intrinsically different light-curve shape-corrected peak luminosities. Additionally, for the CDFs to have the same

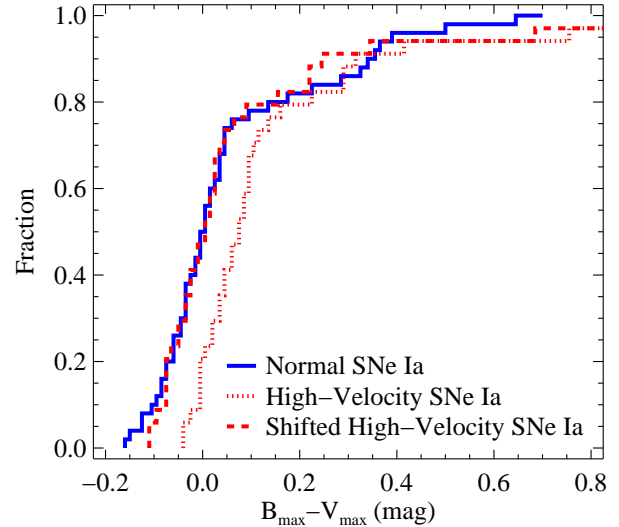


FIG. 5.— $B_{\max} - V_{\max}$ CDF for the Normal (blue solid line), raw High-Velocity (red dotted line), and High-Velocity shifted by -0.07 mag (red dashed line) subsamples. All SNe Ia shown here have $1 \leq \Delta m_{15}(B) \leq 1.5$ mag.

shape, but be offset in color, the High-Velocity SNe Ia must have an additional amount of dust corresponding to $E(B - V)_{\text{host}} \approx 0.07$ mag for all values of $B_{\max} - V_{\max}$. Alternatively, a difference in intrinsic color accounts for the offset in the CDFs and does not require a difference in the light-curve shape-corrected peak luminosities for the two subsamples. The lack of High-Velocity SNe Ia with colors as blue as the bluest Normal SNe Ia is additional evidence that there is almost certainly an intrinsic color difference.

2.4. Properly Measuring R_V for a Sample of Supernovae

Several groups have noted that the Hubble residuals of SNe Ia are minimized by choosing a very low (and potentially unphysical) value of R_V (e.g., Tripp 1998; Astier et al. 2006; Guy et al. 2007; Conley et al. 2007; Kessler et al. 2009; Hicken et al. 2009b; Amanullah et al. 2010). The methods vary in detail, but all are essentially equivalent to fitting a line to the data in a plot like Figure 1 or 2. If SNe Ia have intrinsically different colors, this method ignores critical information.

An example of this problem is shown in Figure 2. We fit the entire sample of SNe Ia with $E(B - V)_{\text{host}} \leq 0.35$ mag from W09 with a single line. Since the Normal subsample has bluer objects for the same M_V than the High-Velocity subsample, this process will naturally reduce the slope of the fit — effectively reducing the value of R_V . Where both the Normal and High-Velocity subsamples are best-fit with $R_V = 2.50$ separately, combined they are best fit by $R_V = 2.21 \pm 0.21$.

If one properly separates these groups, the situation becomes the same as described in Section 2.2. This clearly affects the distances measured in previous cosmological analyses and should be accounted for in the future.

2.5. Improvement to Measured Distances

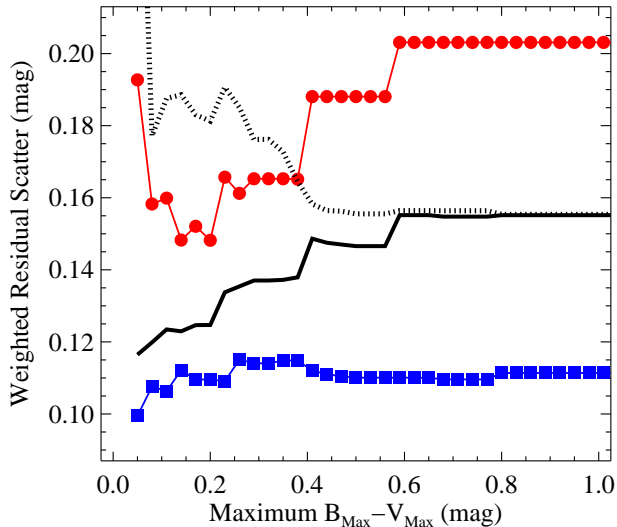


FIG. 6.— Weighted Hubble residual scatter as a function of maximum $B_{\max} - V_{\max}$ color. The dotted and solid lines represent the full sample (with $1 \leq \Delta m_{15}(B) \leq 1.5$ mag) assuming a single intrinsic color and separate intrinsic colors for Normal and High-Velocity SNe Ia, respectively. The blue squares and red circles represent the Normal and High-Velocity subsamples, respectively. Using separate intrinsic colors for the two subsamples significantly reduces the scatter. Additionally, Normal SNe Ia appear to have significantly smaller scatter than High-Velocity SNe Ia.

W09 noted that using a different value of R_V for the two subsamples would reduce the scatter of Hubble residuals for their sample. However, as Section 2.2 showed, the two subsamples have similar values of R_V if the extremely reddened SNe Ia are excluded, and it is not clear that two values of R_V is particularly useful for cosmological samples. In this section, we examine how the Hubble scatter is affected by separating the SNe Ia into two groups based on their ejecta velocity.

Figure 6 presents the weighted residual scatter, defined as

$$\left(\frac{\sum (\Delta\mu^2/\sigma^2)}{\sum (1/\sigma^2)} \right)^{1/2}, \quad (2)$$

where $\Delta\mu$ and σ are the Hubble residual the uncertainty of the distance modulus for a given SN Ia, respectively, for different samples as a function of maximum $B_{\max} - V_{\max}$ color. In the figure, the full sample (with $1 \leq \Delta m_{15}(B) \leq 1.5$ mag) is represented by the black lines, while the Normal and High-Velocity subsamples are represented by blue squares and red circles, respectively. The fits which generate the black dotted line assume a single intrinsic color for the entire sample, and allow M_{zp} and R_V to vary for each maximum value of $B_{\max} - V_{\max}$. This is the approach that has normally been used in cosmological analyses. To determine the scatter for the other samples, all parameters were fixed for all maximum values of $B_{\max} - V_{\max}$, and only a color offset between the Normal and High-Velocity SNe Ia was applied.

For $B_{\max} - V_{\max} \leq 1$ mag, the scatter is consistently improved by using two intrinsic colors. For SNe Ia with $B_{\max} - V_{\max} \leq 0.2$ mag (corresponding to $E(B - V) \lesssim 0.3$ mag and $A_V \lesssim 0.7$ mag), the scatter decreases from

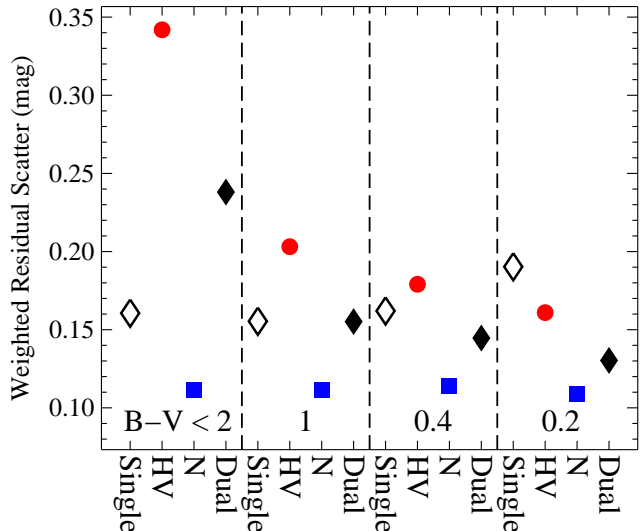


FIG. 7.— Weighted Hubble residual scatter as a function of maximum $B_{\max} - V_{\max}$ color for various samples and methods. The empty and filled black diamonds represent the full sample (with $1 \leq \Delta m_{15}(B) \leq 1.5$ mag) assuming a single intrinsic color (labeled ‘Single’) and separate intrinsic colors (labeled ‘Dual’) for Normal and High-Velocity objects, respectively. The blue squares and red circles represent the Normal (labeled ‘N’) and High-Velocity (labeled ‘HV’) subsamples, respectively. Only the values for $B_{\max} - V_{\max} \leq 0.2, 0.4, 1,$ and 2 mag (from right to left) for each sample and method are plotted.

0.190 mag to 0.130 mag by adopting this method. Furthermore, the Normal subsample has a scatter of only 0.109 mag for this color cut. This is better visualized in Figure 7, where only a subset of the data from Figure 6 is plotted.

Increasing the maximum color increases the scatter of the High-Velocity subsample, but the scatter of the Normal subsample remains constant for all color ranges. This is a consequence of the Normal subsample having a single value for R_V for all colors while the High-Velocity SNe Ia have a significantly different value for R_V depending on the maximum color (see Section 2.2 and Figure 3). This, in turn, increases the scatter of the full sample for large values of $B_{\max} - V_{\max}$, even when using different intrinsic colors for the subsamples. Perhaps counterintuitively, the scatter of the full sample with a single intrinsic color increases as the maximum color is decreased. This is mostly because the fraction of Normal to High-Velocity SNe Ia increases with increasing color in our sample.

Despite the relatively small number of High-Velocity SNe in this sample, it is noteworthy that the Normal SNe have a significantly better Hubble residual scatter — *even after treating each subsample separately*. A future study may find a color parameter that scales with velocity, rather than a simple splitting of the sample, will help improve this measurement. But in the era of large SN samples, where systematic uncertainties are larger than statistical uncertainties and the sample sizes are large enough to choose the “best” objects, using only Normal SNe Ia for measuring cosmological parameters may be a prudent choice. Of course it goes without saying that such a selection (at least at this time) would require a spectrum.

Our analysis is relatively simplistic. Peak absolute magnitudes are corrected for light-curve shape using only a linear relationship with $\Delta m_{15}(B)$, the reddening estimate is derived essentially only from $B_{\max} - V_{\max}$, and the distance moduli are derived from peak absolute magnitudes in a single band (V). Furthermore, the SN Ia sample is split by velocity rather than having a model with velocity as a parameter (this is currently necessary since W09 has not released their $v_{\text{Si II}}$ measurements). Nonetheless, this initial analysis provides the foundation for more sophisticated analyses. In particular, $v_{\text{Si II}}$ (or perhaps a more general ejecta velocity parameter) appears to be a true “second parameter” which significantly improves the precision with which we can measure distances to SNe Ia beyond that of just light-curve shape and color.

3. THEORETICAL UNDERSTANDING

Thus far, empirical relationships between ejecta velocity and intrinsic color have been presented. In this section, we present a simple explanation for these correlations. We then suggest that this scenario is a natural prediction of asymmetric SN explosions. Finally, we show that a set of model light curves and spectra also show a correlation between color and ejecta velocity.

3.1. A Toy Model

An extremely simplistic model of a SN SED near maximum brightness is the following: a blackbody spectrum is generated from electron scattering in the ejecta, imprinted on this spectrum are broad P-Cygni lines from strong lines, and this causes significant absorption at wavelengths shorter than $\sim 4300 \text{ \AA}$, where line-blanketing from Fe-group elements is significant. The wavelength where line opacity and electron-scattering opacity are similar is at $\sim 4300 \text{ \AA}$ (Kasen & Woosley 2007), which is near the peak of the B band.

As ejecta velocity increases, one expects the width of line-forming regions in velocity space to increase (i.e., at higher velocities, lines get broader); this is especially true for saturated lines. Therefore, individual lines overlap more for higher-velocity ejecta. For wavelengths dominated by electron scattering, this should not significantly affect the SED. However, for regions where line opacity is dominant, or in regions where the two effects are of similar strength, higher velocities should increase the opacity. Since the B band is a region where the line and electron-scattering opacities are of similar strength, the B -band flux should decrease with higher velocity. However, the V band, which is in a region dominated by electron scattering, will be less affected by higher ejecta velocity, and the V -band flux should not change significantly. Therefore, one *expects* that higher ejecta velocity should result in a redder $B - V$ color.

SN ejecta have a negative temperature gradient with radius. Since the outer layers are cooler, SNe with higher velocities will have more absorption from lower excitation (e.g., Fe II vs. Fe III) lines. Because of the larger number of optical lines for the lower excitation states, higher-velocity ejecta should produce additional line blanketing at blue wavelengths. Again, one *expects* that higher ejecta velocity should result in a redder $B - V$ color.

This has been shown in some theoretical models. KP07 generated light curves and spectra for a single asymmet-

ric SN Ia explosion model from different lines of sight. The asymmetry of the KP07 model is the result of a surface detonation, but the final ejecta distribution is qualitatively similar to that of general off-center explosions, resulting either from off-center ignition or detonation conditions, or both (e.g., Maeda et al. 2010a). The asymmetry of the model is not (at this point) important for the discussion, but it allows an examination of SNe Ia with different ejecta velocities for the same explosion energy. There is a clear correlation between viewing angle and both $v_{\text{Si II}}$ and $B - V$ at maximum light. Although this was not explicitly mentioned by KP07, the different lines of sight showed that with increasing $v_{\text{Si II}}$ the $B - V$ color became redder. This is a validation of the simple explanation presented above.

There are several ways to generate different ejecta velocities for a given luminosity, but this is also a natural outcome of an asymmetric explosion, where different viewing angles have similar luminosities but vastly different ejecta velocities. Multi-dimensional theoretical models of SN Ia explosions have shown that they can be highly asymmetric (e.g., Reinecke et al. 2002; Gamezo et al. 2005; Kuhlen et al. 2006). Further theoretical models have shown that the asymmetry can significantly affect observables depending on viewing angle (Kasen et al. 2009). From this work, it is expected that SNe Ia be asymmetric and that the asymmetry to increase the dispersion of SN distances, which in turn decreases the precision with which SNe Ia can constrain cosmological parameters.

Spectropolarimetry of SNe Ia has shown that most SNe Ia have very low continuum polarization, but can have significant line polarization, especially in the Si II $\lambda 6355$ feature (e.g., Leonard et al. 2005; Wang et al. 2007; see Wang & Wheeler 2008 for a review). Spectropolarimetry probes asymmetries of the SN in the plane of the sky. The data suggest that the global asymmetry of a SN Ia is typically $\lesssim 10\%$, but that a large plume of Si-rich material with a preferred axis may be present in all SNe Ia. Wang et al. (2007) also presented tantalizing evidence that the light-curve shape of a SN Ia is correlated with the amount of polarization in the Si II feature.

Recently, Maeda et al. (2010b) found that there were significant offsets from zero velocity for relatively unblended forbidden lines in the nebular spectra of SNe Ia. These lines probe the inner ejecta of the SN, and if the explosion were symmetric, one would expect them to be centered at zero velocity. Maeda et al. (2010a) found a striking correlation between the velocity offsets of these features and the velocity gradient of the Si II $\lambda 6355$ feature, $\dot{v}_{\text{Si II}}$, at early times. This observation connects the outer layers of the ejecta to the explosion near the center of the star, and suggests an intrinsically asymmetric explosion mechanism for the majority of SNe Ia. Maund et al. (2010) also found a correlation between the amount of polarization in the Si II feature and $\dot{v}_{\text{Si II}}$, suggesting that $\dot{v}_{\text{Si II}}$ is an excellent probe of asymmetry of the outer layers of the SN ejecta.

Our work also fits within this framework. Intrinsic color correlates with $v_{\text{Si II}}$, which correlates with $\dot{v}_{\text{Si II}}$. Since $\dot{v}_{\text{Si II}}$ does not correlate with luminosity, we require two explosions with similar luminosities to have vastly different ejecta velocities. That is naturally explained if

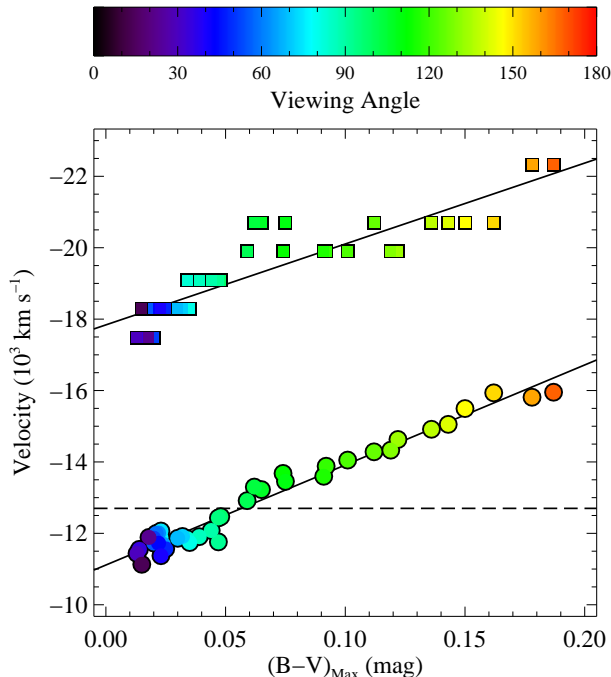


FIG. 8.— Maximum-light Si II $\lambda 6355$ (circles) and Ca H&K (squares) velocity as a function of maximum-light $B - V$ color for the KP07 model spectra. Each viewing angle is represented by a different color with the mapping shown by the color bar at the top. The best-fit lines for each feature are shown as black solid lines. The dashed line represents the $v_{\text{Si II}}$ offset from the mean of the Normal velocity clump that W09 used to differentiate the Normal and High-Velocity subsamples. It also roughly separates viewing angles into two hemispheres.

SNe Ia are asymmetric with all lines of sight having a similar luminosity but some lines of sight showing significantly different ejecta velocities than others.

3.2. Model Light Curves & Spectra

The KP07 models can be used to examine correlations between various observables with the hope of understanding the physics behind our empirical findings. KP07 already noted that $B - V$ color evolution and $v_{\text{Si II}}$ depend on viewing angle. However, they did not examine the maximum-light values of these two quantities and their correlation. Figure 8 shows the $(B - V)_{\text{max}}$ color and $v_{\text{Si II}}$ as a function of viewing angle. The two values are highly correlated, and a linear fit produces

$$v = (-11.1 - 28.0(B - V)_{\text{max}}) \times 10^3 \text{ km s}^{-1}. \quad (3)$$

A similar relationship exists for the Ca H&K feature, with

$$v = (-17.8 - 22.7(B - V)_{\text{max}}) \times 10^3 \text{ km s}^{-1}. \quad (4)$$

Not surprisingly, the velocity of the Si and Ca features are highly correlated in the models. However, unlike the Si II $\lambda 6355$ feature, which was fit with a Gaussian to determine the minimum of the feature, the Ca H&K feature had a very complex profile for some viewing angles, and the velocity was simply measured from the minimum of the profile. Thus the precision of this measurement is limited by the resolution of the model spectra. Real SN Ia data show complex, non-Gaussian line profiles with multiple absorption minima for the Ca H&K

feature (e.g., Branch et al. 2006). This is further complicated by varying quality for each observed spectrum. Future work should determine if Ca H&K correlates with color in a manner similar to Si II.

While our toy model and the models of KP07 predict that $B_{\text{max}} - V_{\text{max}}$ monotonically increases with ejecta velocity, our current analysis simply splits the sample into two groups based on $v_{\text{Si II}}$. Future studies should determine from the data if a linear relationship is more appropriate. This simplification may also be why the Hubble scatter is larger for the High-Velocity subsample than the Normal subsample. Additionally, the velocity used to separate the samples is somewhat arbitrary and there could be some blending between the samples, leading to an increase in the Hubble residual scatter. A linear relationship would avoid such a potential bias.

W09 found that the Normal SNe Ia had a mean value of $\langle v_{\text{Si II}} \rangle \approx -10,600 \text{ km s}^{-1}$, and a value of $v_{\text{Si II}} \approx -11,800 \text{ km s}^{-1}$ was used to split the sample into the two subsamples. Using the same velocity difference from the mean to separate the KP07 model spectra (the lower-velocity clump is at $v_{\text{Si II}} \approx -11,500 \text{ km s}^{-1}$, so the separation would be at $v_{\text{Si II}} \approx -12,700 \text{ km s}^{-1}$), the velocity separation also cleanly separates the models into a lower-velocity clump and a higher-velocity tail. Interestingly, this separation also almost perfectly separates the viewing angles into two hemispheres. The KP07 model colors are also systematically redder than the observations, but this trend is typical of other light curve models (e.g., Kasen et al. 2009; Kromer & Sim 2009) and is likely due to the neglect of non-local thermodynamic equilibrium effects in the radiation transport calculations.

Though the analysis here was done with a single aspherical model, the same sorts of effects can be seen in spherical models when the explosion energy is varied for a given ^{56}Ni mass. We have examined the survey of parameterized 1-D models of Woosley et al. (2007) and confirmed that a higher kinetic energy results in a redder color at peak.

4. DISCUSSION & CONCLUSIONS

We have re-analyzed a large sample of SN Ia data originally presented by W09. We have verified the results of W09: after splitting the sample by $v_{\text{Si II}}$, the two subsamples have different relationships between the light-curve shape-corrected (but not host-galaxy extinction-corrected) peak magnitude and color excess, and that difference can be explained with different reddening laws for the subsamples. However, we find that this conclusion no longer holds when the reddest SNe Ia are excluded from the sample, and in this regime, both subsamples can be described by the same reddening law. Furthermore, the two subsamples are offset from each other in the plane of color and absolute magnitude. Since the bluest High-Velocity SNe Ia are significantly redder than the bluest Normal SNe Ia (also noticed by W09) and the CDFs of the two subsamples have the same shape, but are also offset in color, we conclude that the two subsamples have different intrinsic colors.

This result has significant implications for SN Ia cosmology. First, by assuming a single intrinsic color for all SNe Ia, one will naturally find a smaller value for R_V than if the subsamples are treated separately. Second, assuming a single intrinsic color could significantly bias

cosmological results, particularly if the fraction of Normal to High-Velocity SNe Ia changes with redshift, which may have already been seen in data (Kessler et al. 2009). Finally, we find that the scatter in the Hubble residuals for SNe Ia with $B_{\max} - V_{\max} \leq 0.2$ mag is reduced from 0.190 mag to 0.130 mag by using two separate intrinsic colors for the velocity subsamples. The Hubble scatter is further reduced to 0.109 mag by exclusively using the Normal subsample. To perform this measurement, a single spectrum within a week of maximum brightness is required.

The correlation between ejecta velocity and color can naturally be explained by additional line blanketing for the higher-velocity SNe Ia, affecting the SED in the B band, but leaving the V band not as greatly affected. We show that a simple asymmetric explosion model can reproduce the general trends in the data.

The relationship between ejecta velocity and intrinsic color will be a significant tool for measuring extremely precise distances with SNe Ia. Better theoretical understanding of this relationship and additional observational investigations are necessary to fully leverage this finding. It is also important to incorporate this information into existing SN Ia distance estimators, which currently depend solely on light-curve information. We have only investigated color near maximum-brightness, and it is important to see how ejecta velocity correlates with color at

all phases — especially at late phases when SNe Ia are assumed to have the same intrinsic color regardless of light-curve shape (Lira et al. 1998). If future surveys want the most precise SN Ia distances possible, they should have a significant spectroscopic component. This is particularly important for the design of WFIRST, where a decision must be made regarding whether a spectrograph (and with what resolution) should be included.

R.J.F. is supported by a Clay Fellowship.

R.J.F. would like to thank the many people with whom he discussed this study. In particular, R. Kirshner, P. Mazzali, M. Phillips, S. Jha, K. Mandel, S. Hachinger, W. Li, X. Wang, and F. Röpke, and S. Blondin influenced the direction of this work. Part of the analysis occurred at the Aspen Center for Physics during the Summer 2010 workshop, “Taking Supernova Cosmology into the Next Decade.” Additional analysis occurred while visiting the Max-Planck-Intitut für Astrophysik. R.J.F. would especially like to thank W. Hillebrandt for his support during this stay. The environment that he, along with P. Mazzali, F. Röpke, and the numerous postdoctoral and graduate students have generated is extremely stimulating.

REFERENCES

- Amanullah, R., et al. 2010, *ApJ*, 716, 712
 Astier, P., et al. 2006, *A&A*, 447, 31
 Bailey, S., et al. 2009, *A&A*, 500, L17
 Benetti, S., et al. 2005, *ApJ*, 623, 1011
 Branch, D., et al. 2006, *PASP*, 118, 560
 Branch, D., Fisher, A., & Nugent, P. 1993, *AJ*, 106, 2383
 Conley, A., Carlberg, R. G., Guy, J., Howell, D. A., Jha, S., Riess, A. G., & Sullivan, M. 2007, *ApJ*, 664, L13
 Conley, A., et al. 2008, *ApJ*, 681, 482
 Elias-Rosa, N., et al. 2006, *MNRAS*, 369, 1880
 Filippenko, A. V. 1997, *ARA&A*, 35, 309
 Filippenko, A. V., et al. 1992a, *AJ*, 104, 1543
 ——. 1992b, *ApJ*, 384, L15
 Foley, R. J., et al. 2009, *AJ*, 138, 376
 Foley, R. J., Filippenko, A. V., & Jha, S. W. 2008, *ApJ*, 686, 117
 Foley, R. J., Narayan, G., Challis, P. J., Filippenko, A. V., Kirshner, R. P., Silverman, J. M., & Steele, T. N. 2010, *ApJ*, 708, 1748
 Gamezo, V. N., Khokhlov, A. M., & Oran, E. S. 2005, *ApJ*, 623, 337
 Goobar, A. 2008, *ApJ*, 686, L103
 Guy, J., et al. 2007, *A&A*, 466, 11
 Guy, J., Astier, P., Nobili, S., Regnault, N., & Pain, R. 2005, *A&A*, 443, 781
 Hicken, M., et al. 2009a, *ApJ*, 700, 331
 Hicken, M., Wood-Vasey, W. M., Blondin, S., Challis, P., Jha, S., Kelly, P. L., Rest, A., & Kirshner, R. P. 2009b, *ApJ*, 700, 1097
 Howell, D. A., et al. 2006, *Nature*, 443, 308
 Jeffery, D. J., Leibundgut, B., Kirshner, R. P., Benetti, S., Branch, D., & Sonneborn, G. 1992, *ApJ*, 397, 304
 Kasen, D., & Plewa, T. 2007, *ApJ*, 662, 459
 Kasen, D., Röpke, F. K., & Woosley, S. E. 2009, *Nature*, 460, 869
 Kasen, D., & Woosley, S. E. 2007, *ApJ*, 656, 661
 Kessler, R., et al. 2009, *ApJS*, 185, 32
 Krisciunas, K., Hastings, N. C., Loomis, K., McMillan, R., Rest, A., Riess, A. G., & Stubbs, C. 2000, *ApJ*, 539, 658
 Kromer, M., & Sim, S. A. 2009, *MNRAS*, 398, 1809
 Kuhlen, M., Woosley, S. E., & Glatzmaier, G. A. 2006, *ApJ*, 640, 407
 Leibundgut, B., et al. 1993, *AJ*, 105, 301
 Leonard, D. C., Li, W., Filippenko, A. V., Foley, R. J., & Chornock, R. 2005, *ApJ*, 632, 450
 Li, W., et al. 2003, *PASP*, 115, 453
 ——. 2001, *PASP*, 113, 1178
 Lira, P., et al. 1998, *AJ*, 115, 234
 Maeda, K., et al. 2010a, *Nature*, 466, 82
 Maeda, K., Taubenberger, S., Sollerman, J., Mazzali, P. A., Leloudas, G., Nomoto, K., & Motohara, K. 2010b, *ApJ*, 708, 1703
 Maund, J. R., et al. 2010, *ArXiv e-prints*, 1008.0651
 Nugent, P., Phillips, M., Baron, E., Branch, D., & Hauschildt, P. 1995, *ApJ*, 455, L147
 Perlmutter, S., et al. 1999, *ApJ*, 517, 565
 Phillips, M. M. 1993, *ApJ*, 413, L105
 Reinecke, M., Hillebrandt, W., & Niemeyer, J. C. 2002, *A&A*, 391, 1167
 Riess, A. G., et al. 1998, *AJ*, 116, 1009
 Riess, A. G., Press, W. H., & Kirshner, R. P. 1996, *ApJ*, 473, 88
 Riess, A. G., et al. 2007, *ApJ*, 659, 98
 Stritzinger, M., Mazzali, P. A., Sollerman, J., & Benetti, S. 2006, *A&A*, 460, 793
 Tripp, R. 1998, *A&A*, 331, 815
 Wang, L., Baade, D., & Patat, F. 2007, *Science*, 315, 212
 Wang, L., & Wheeler, J. C. 2008, *ARA&A*, 46, 433
 Wang, X., et al. 2009, *ApJ*, 699, L139
 ——. 2008, *ApJ*, 675, 626
 Wood-Vasey, W. M., et al. 2007, *ApJ*, 666, 694
 Woosley, S. E., Kasen, D., Blinnikov, S., & Sorokina, E. 2007, *ApJ*, 662, 487